ACS Partner Journal

ENVIRONMENT & HEALTH

Open Access

pubs.acs.org/EnvHealth

Article

Lung Single-Cell Transcriptomics Offers Insights into the Pulmonary Interstitial Toxicity Caused by Silica Nanoparticles

Yan Li, Qing Yao, Hailin Xu, Jiaze Ren, Yurou Zhu, Caixia Guo,* and Yanbo Li*

Cite This: *Environ. Health* 2024, 2, 786−801

Read Online

ACCESS | Metrics & More | Article Recommendations | Supporting Information

ABSTRACT: The adverse respiratory outcomes motivated by silica nanoparticles (SiNPs) exposure have received increasing attention. Herein, we aim to elucidate the interplay of diverse cell populations in the lungs and key contributors in triggering lung injuries caused by SiNPs. We conducted a subchronic respiratory exposure model of SiNPs *via* intratracheal instillation in Wistar rats, where rats were administered with 1.5, 3.0, or 6.0 mg/kg body weight SiNPs once a week for 12 times in total. We revealed that SiNPs caused pulmonary interstitial injury in rats by histopathological examination and pulmonary hydroxyproline determination. Further, a single-cell RNA-Seq *via* screening 10 457 cells in the rat lungs disclosed cell-specific responses to SiNPs and cell-to-cell interactions within the alveolar macrophages, epithelial cells, and fibroblasts from rat lungs. These disturbed responses were principally related to the dysregulation of protein homeostasis (proteostasis), accompanied by an inflammatory response in macrophages, cell death in epithelial, proliferation, and extracellular matrix deposition in fibroblast. These cell-specific responses may serve a synergistic role in the pathogenesis of pulmonary interstitial disease triggered by SiNPs. In particular, the analyses of gene interaction networks and gene−disease associations filtered out heat shock proteins (Hsps) family genes crucial to the observed pulmonary lesions caused by SiNPs. Of note, both GEO database analysis and our experiments' validation indicated that Hsps, especially Hspd1, may be a key contributor to pulmonary interstitial injury, possibly through triggering oxidative stress, immune response, and disrupting protein homeostasis. Taken together, our study provides insights into pulmonary toxic effects and underlying molecular mechanisms of SiNPs from a single-cell perspective.

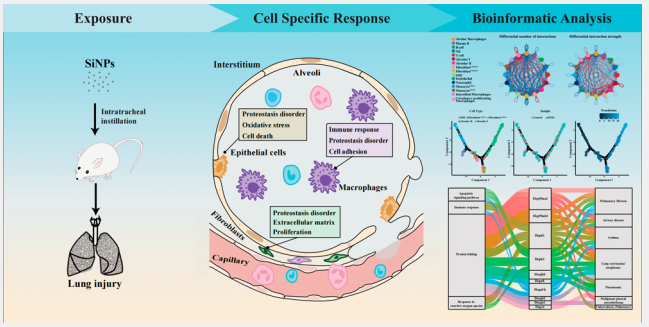

KEYWORDS: *silica nanoparticles, single-cell RNA-Seq, lung toxicity, lung interstitial disease, proteostasis*

1. INTRODUCTION

Due to excellent physical and chemical properties and the development of nanotechnology, silica nanoparticles (SiNPs) have been applied in more and more extensive fields, such as industrial manufacture, biological medicine, and food additives.[1] Meanwhile, SiNPs and their related products were inevitably released into the environment in large quantities, thus resulting in increased environmental burden and risks to human health.[2] Especially, the nanohandling workers and nanoproduct consumers would stand at the forefront of exposure. SiNPs were listed as one of the priority nanomaterials for toxicity evaluation by the Organisation for Economic Cooperation and Development, OECD.[3] Nevertheless, the updated risk management and safety evaluation of SiNPs still lag far behind the development of nanotechnology. Accumulating research has illustrated some pathological diseases attributed to SiNPs exposure, including impairments in respiratory, cardiovascular, reproductive, digestive, and neurological systems.[4−9] However, many issues regarding its adverse effects, in particular cell-specific responses, potential functional actions, and molecular mediators, remain not yet answered.

There is ample evidence to disclose the lung as the preliminary target site upon the inhalation of SiNPs, especially in the occupational scenario.[10,11] For example, a series of *in vivo* and *in vitro* experimental investigations have reported that SiNPs could promote pulmonary inflammation, asthma, chronic obstructive pulmonary disease (COPD), pulmonary fibrosis, and even cancer.[12−17] Also, epidemiological evidence has shown that exposure to SiNPs resulted in prominent changes in the antioxidant enzyme (GPX) and lung function (forced expiratory flow at 25%, FEF25%) during the 6-month followup of the workers.[18] Nevertheless, the related pathogenesis, cellular or tissue response, cell-to-cell association, and underlying mechanisms for the pathological pulmonary lesions upon inhaled SiNPs stimuli still need to be further explored.

Received: March 5, 2024
Revised: June 8, 2024
Accepted: June 11, 2024
Published: July 1, 2024

https://doi.org/10.1021/envhealth.4c00052
Environ. Health 2024, 2, 786−801

Based on next-generation sequencing technology (RNA-Seq), some investigators have certified transcriptome at the organ level in the human body.[19] However, it only presented the average expression of all cells and cloaked the state of single cells or certain cell clusters in the sample. An in-depth study on the transcriptional status of individual cells is needed. Single-cell RNA sequencing (scRNA-seq), an essential branch of system biology, describes the transcriptome landscape and provides a deeper picture of injury or disease based on cellular-level features from a cellular mapping perspective.[20,21] Moreover, it can recognize known or novel cell populations, reliably identify the closely related cell populations and heterogeneity of gene expression, and then analyze the cell populations at the single-cell level under physiological and pathological conditions.[22,23] According to the literature, the lung is a highly complex organ comprised of more than 58 cell populations in the body,[24,25] including epithelial cells, endothelial cells, immune cells, stromal cells, fibroblasts, and various subtypes evolved from these cells and their crosstalk. Currently, the cellular crosstalk and cell-specific response in the adverse outcomes of SiNPs in lungs remain largely unknown. In this context, by using single-cell Seq, we comprehensively evaluated the changes of individual cell clusters and gene expressions in rat lungs with a 3-month repeated SiNPs exposure. Our data would allow us to clarify the complex cellular interactions and identify underlying molecular mechanisms contributing to SiNPs-induced pulmonary toxicity, which may help in assessing the health risks of SiNPs and benefit the safety development of nanotechnology.

2. METHODS AND MATERIALS

2.1. Animal Studies

Male Wistar rats (6-week old) were obtained from China Vital River Laboratory Animal Technology Co., Ltd., and maintained in the specific pathogen-free (SPF) animal facility of Capital Medical University. After 1 week of adaption, the rats were randomly divided into four groups (one control and three SiNPs groups) and administered 0.9% saline (control rats) or SiNPs suspension (1.5, 3.0, or 6.0 mg/kg body weight (bw)) *via* intratracheal instillation. The treatment was provided with the controlled volume at 200 ± 20 μL once every 7 days for 12 times in total. The experimentation was terminated after a 6-week interval from the last particle administration. Lastly, the rats were fasted overnight, lung samples were harvested and weighed, and the organ coefficient was calculated. SiNPs were synthesized using the Stöber approach, and their characterization was previously described.[15] The administered dosage was set based on the permissible concentration of amorphous SiO_2 (5 mg/m^3) in the workplace and the respiration physiology of the rat (0.86 mL/breath, 85 breaths/min). The animal experiment was approved by the Animal Care and Use Committee at Capital Medical University (ethical number: AEEI-2021-088).

2.2. Histopathological Examination

Fresh lung tissue was immersed in 4% paraformaldehyde solution for 24 h and embedded into paraffin. Then, the lung sections were stained with hematoxylin and eosin (HE; Jiancheng, China) and Masson's trichrome (Jiancheng, China) for lung histopathological assessment. All lung sections were digitized by scanning using the automatic slice scanning system (3D HISTECH, Hungary) and analyzed in ImageJ. Moreover, the scoring of lung injury was done using the Ashcroft scale.

2.3. Hydroxyproline (HYP) Assay

HYP is a sensitive indicator of collagen deposition and fibrosis. Its lung level was analyzed by a Hydroxyproline Assay Kit (Jiancheng, China) based on the product manual.

2.4. scRNA-seq

2.4.1. Experiment Process. After collection, the fresh lung tissues from the control and 6.0 mg/kg bw SiNPs groups were washed with ice-cold RPMI1640 (Gibco, UK), dissociated using Multitissue dissociation kit 2 (Miltenyi, Germany), and erythrocytes removed by red blood cell lysis solution (Miltenyi, Germany) in order according to the instructions. Cell number and viability were estimated by a fluorescent cell analyzer (Countstar Rigel S2), and cell viability was above 95%; then, the fresh cells were washed in the RPMI1640 (Gibco, UK) and resuspended in phosphate buffer saline (PBS; Gibco, UK) and bovine serum albumin at 1×10^6 cells/mL. Next, library preparation was performed by using a SeekOne Digital Droplet Single Cell 3′ library preparation kit (SeekGene, China). Fastp (v0.20.1)[26] was employed to trim primer sequence and low-quality bases of raw reads and then gather the original statistics.

2.4.2. Processing Data and Clustering Markers. The Seekone Tools pipeline was used to process the cleaned reads and generate the transcript expression matrix. We excluded cells with less than 300 detected genes. Then, the mitochondria gene expression was calculated *via* the Seurat package's percentage feature set function. To eliminate low-activity cells, we excluded cells expressing mitochondria genes with over 26.18% and 24.41%, respectively, in the control and SiNPs group. The filtered data were used to apply subsequent analyses. We normalized the data and completed the visualization *via* clustering with Uniform Manifold Approximation and Projection (UMAP) by the Seurat R package.

2.4.3. Cell−Cell Communication Analysis. Cell−cell communication analysis was conducted using the CellChat R package to investigate potential interactions among cell subsets in the rat lungs. In brief, specific cell−cell communication was inferred by recognizing differentially signaling genes (p value < 0.05) and ligands and receptors in clusters. Subsequently, signaling pathways, influences, and more information were obtained from network analysis, which were displayed with a circle plot.

2.4.4. Analysis of Gene Differential Expression and Pathway. The threshold set for up- and downregulated differential expression genes (DEGs) was adjusted to p value less than 0.05 by Bonferroni. DEGs showed up on the heatmap. Functional enrichments by Gene Ontology (GO) and Kyoto Encyclopedia of Genes and Genomes (KEGG) analysis were performed. Then, GO chords were employed to connect the vital DEGs and corresponding enriched GO pathways using the circlize package of R. The pathways with corrected p value less than 0.05 by Bonferroni and DEGs with fold change (|FC|) > 2 were considered significantly enriched. To filter out the key genes, gene interaction networks were visualized *via* String and Cytoscape. The top genes were ranked by the Maximal Clique Centrality (MCC) method. Then, the relationship of these genes to lung-related disease was analyzed *via* the DisGeNET platform. Moreover, key gene expressions were extracted by the Seurat package and visualized through the ggplot2 and dplyr package.

2.4.5. Single-Cell Trajectory Analysis. Trajectory analysis was conducted by the Monocle R package to order single cells in "pseudotime".[27] The trajectory of a treelike structure in the dimensional space was visualized, including branches and tips.

2.5. Quantitative Reverse Transcription-Polymerase Chain Reaction (qRT-PCR)

The total RNA extracted from pulmonary tissues was applied to process the qRT-PCR analysis. 1000 ng of total RNA was reversely transcribed to cDNA using PrimeScriptTM RT Master Mix (Takara, Japan), and real-time PCR was carried out in a quantitative thermal cycler (Bio-Rad, USA) using SYBR Premix Ex Taq II (Takara, Japan). Relative gene expression was normalized to β-actin. Primers are listed in the supplementary file, Table S1.

2.6. mRNA Array Analysis

Referring to the gene expression profile of patients with pulmonary interstitial disease in the Gene Expression Omnibus (GEO) database (GSE92592), gene expressions of the Hsps family genes were

https://doi.org/10.1021/envhealth.4c00052
Environ. Health 2024, 2, 786−801

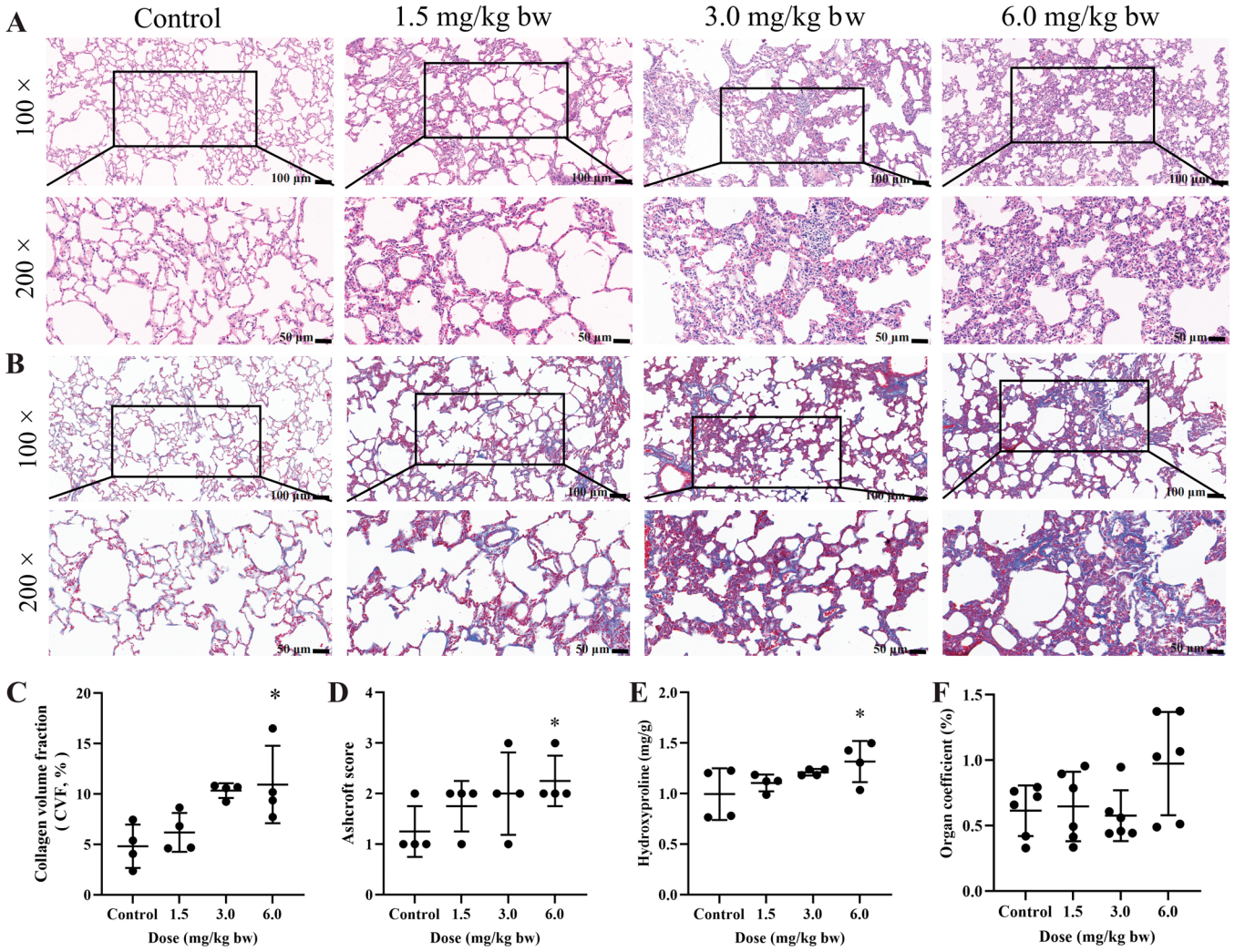

Figure 1. Lung injury induced by SiNPs. (A) HE staining showed a thickened alveolar wall (n = 4). Masson staining (B) and its semiquantitative analysis (C) manifested a dose-dependent increase in collagen deposition. n = 4; magnification, 100× or 200× ; scale bar, 50 or 100 μm. (D) Ashcroft score analysis suggested pulmonary injury caused by SiNPs (n = 4). (E) HYP, as an indicator for collagen hyperplasia, was greatly aggravated in the high-dose (6.0 mg/kg bw) SiNPs exposure group (n = 4). (F) Organ coefficient of the lung (n = 6). *p < 0.05, compared with control.

analyzed by limma packages. Then, the nomogram was used to predict disease onset or progression through multiple indicators.

2.7. Cell Culture and Treatment

For investigating the impact of SiNPs on epithelial, macrophage, and fibroblast cells *in vitro*, BEAS-2B cells (Cell Resource Center; Shanghai, China), PMA-activated THP-1 cells (Peking Union Medical College; Beijing, China), and MRC-5 cells (Cell Resource of the Chinese Academy of Science; Beijing, China) were utilized and routinely cultured in the cell incubator (Thermo Fisher Scientific, USA). In brief, BEAS-2B cells were cultured in DMEM medium (Corning, USA) containing 10% fetal bovine serum (FBS; Gibco, Australia). THP-1 cells were cultured in RPMI 1640 medium (Procell, China) containing 10% FBS and 100 ng/mL PMA (MedChemExpress, USA) for 48 h (named THP-1-M_Φ). MRC-5 cells were seeded in MEM medium (HyClone, USA) containing 10% FBS and 1% Non-Essential Amino Acids (NEAA; Gibco, USA). When 80% confluency was reached, BEAS-2B or THP-1-M_Φ cells were exposed to SiNPs (0, 12.5, 25, and 50 μg/mL) for 24 h. The dosage selection of SiNPs was in accordance with the corresponding cell viability assessment by MTT assay. The detailed data are shown in Supporting Information Figure S1. The supernatants were collected and filtered with 0.22 μm filter membranes (Millipore, Billerica, USA). Afterward, MRC-5 cells were incubated with the culture supernatants from BEAS-2B cells or THP-1-M_Φ without or with SiNPs (named as SB-Ctr/SB-SiNPs or ST-Ctr/ST-SiNPs) for 24 h.

2.8. Western Blot

Proteins were extracted using the Protein Extraction kit (KeyGEN, China) and quantified by BCA assay (Dingguo, China). The expressions of HSP90AB1, HSPD1, HSPB1, and DNAJA1 were measured and normalized by GAPDH. The images were pictured by the Odyssey CLx Imaging System (Gene Company Limited, Hong Kong) and quantified by ImageJ software.

2.9. Statistical Analysis

Except for the scRNA-seq data, all data were presented as "mean ± standard deviation (SD)", and statistical analysis was performed by SPSS 22.0 software. One-way ANOVA was used to compare more than two groups. Then, the *post hoc* test of the homogeneous data was analyzed by the Dunnett (T) test, while heterogeneous data was analyzed by Dunnett's T3 test. A two-sided p value less than 0.05 was determined as statistically significant. The correlation analysis was performed by the Pearson method *via* corrplot, ggplot2, and tidyverse R packages.

https://doi.org/10.1021/envhealth.4c00052
Environ. Health 2024, 2, 786−801

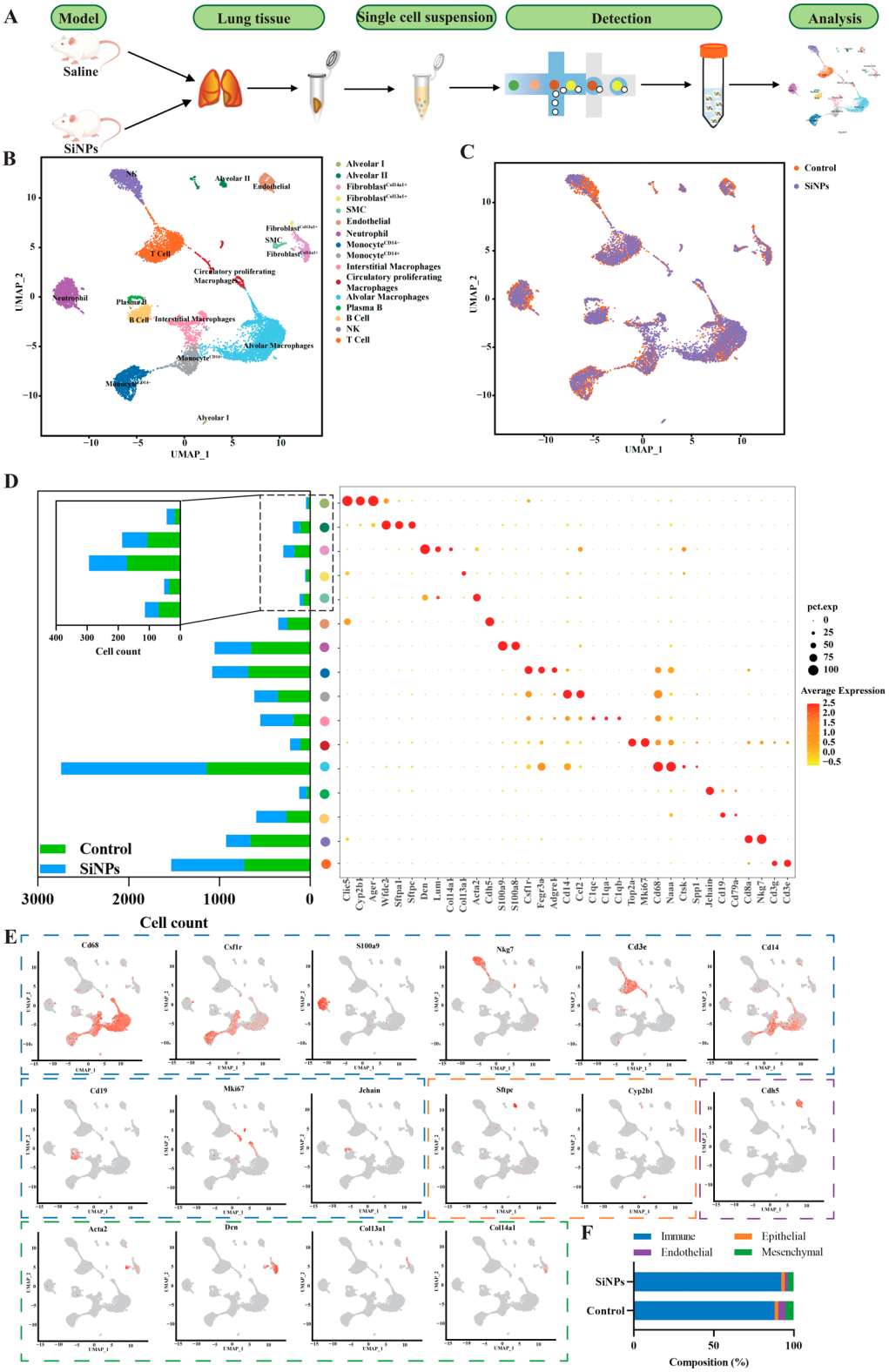

Figure 2. scRNA-seq profiling of the rat lung after SiNPs exposure. (A) Flowchart of the present project. Lung tissues from rats administered with saline or 6.0 mg/kg bw SiNPs were dissociated into single-cell suspensions for subsequent analysis. Cells were clustered and visualized through UMAP, which presented all cells grouped into 16 distinct cell types (B) with the identification of cells from the control and SiNPs group (C). (D) The cell type annotation was based on the canonical marker gene expression (right), and then cell counts of each cluster were calculated per group (left). (E) Canonical markers genes were applied to sign clusters as presented in the UMAP plot. Subsequently, cell types were grouped as immune, epithelial, endothelial, and mesenchymal. (F) The composition percentage of each cell type was analyzed.

https://doi.org/10.1021/envhealth.4c00052
Environ. Health 2024, 2, 786−801

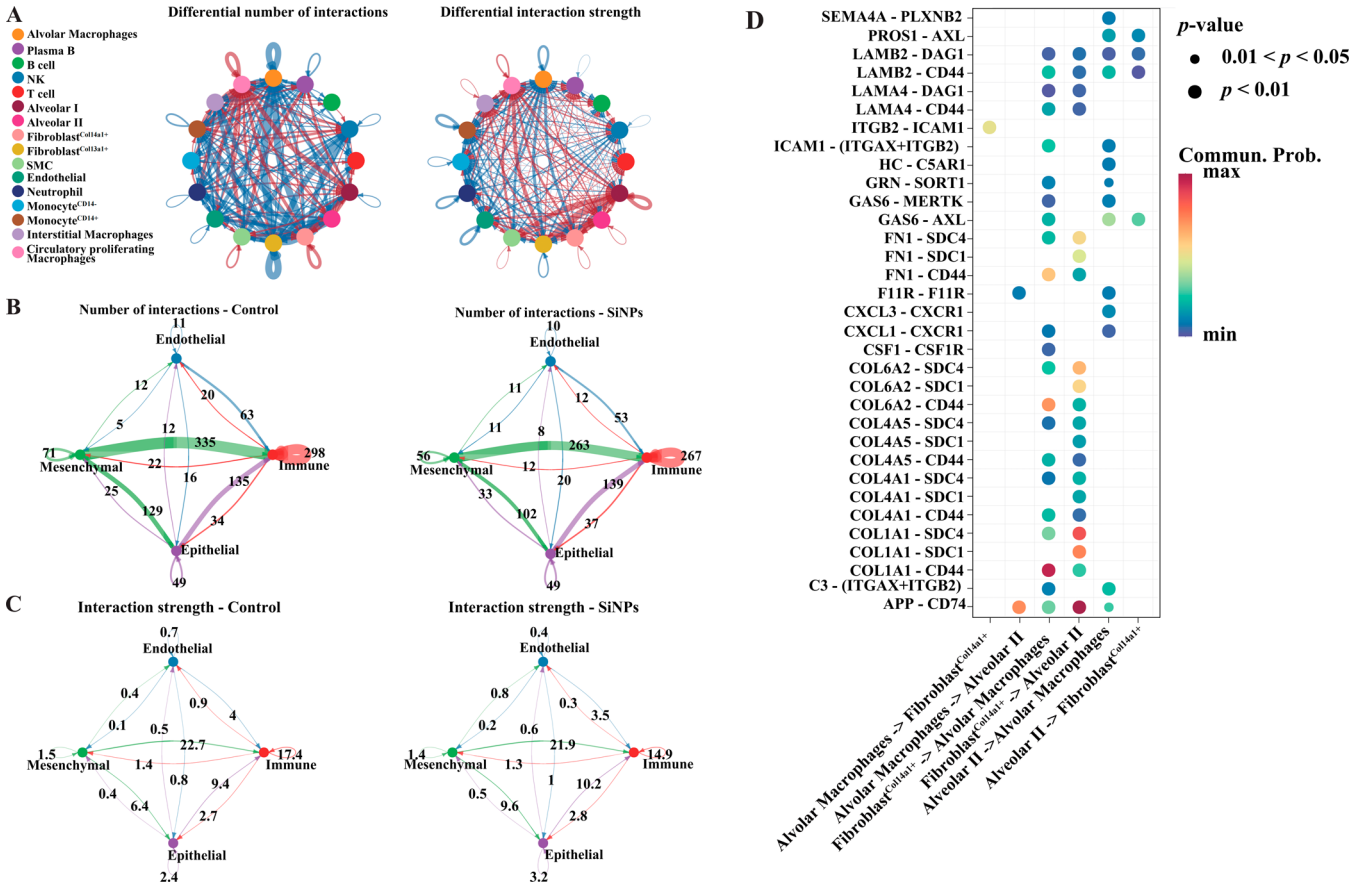

Figure 3. Interaction analysis for cell populations affected by SiNPs in lung tissue. (A) The number and strength of interactions. Line width represents the cognate receptor−ligand pairs. The red or blue lines indicated the up- or downregulation of interaction signals, respectively. (B) Number of intracellular communication between four subgroups. (C) Interaction strength between four subgroups. (D) Ligand−receptor interaction studies.

3. RESULTS

3.1. Pulmonary Toxicity Caused by SiNPs

According to the HE images of lung tissues, partially destroyed alveoli were observed in the lungs of rats exposed to low-dose SiNPs (1.5 mg/kg bw), and thickened alveoli septum was manifested in rats exposed to a higher dose (Figure 1A). Masson staining and its semiquantitative analysis (Figure 1B−C) reflected the collagen deposition in the lung upon SiNPs stimuli. Pathological evaluation of rat lung tissue showed that the score of Ashcroft was dose-dependently increased after SiNPs administration (Figure 1D). Meanwhile, the HYP content was greatly elevated in the SiNPs-exposed lung tissue (Figure 1E). No significant difference was noticed in the organ coefficient of lung (Figure 1F). Taken together, our results illustrated that SiNPs exposure *via* intratracheal instillation induced obvious pathological and interstitial fibrotic alterations in the rat lung.

3.2. scRNA-Seq Identified Cell Types in the Wistar Rat's Lung

In order to explore the impact of SiNPs on the lung across cell types, we applied a scRNA-seq in the rat administered with SiNPs (6.0 mg/kg bw, once per week for 12 times). The details of the experimentation are shown in a flowchart diagram (Figure 2A). In total, 10 457 cells were applied for integrated scRNA-Seq analysis, including 5433 cells from the control lung and 5024 cells from SiNPs-treated rat lung (Figure 2B−C). Sixteen distinct cell types (Figure 2B) were identified based on the expressions of specific markers (Figure 2D−E), including alveolar cells (type I and II), fibroblasts$^{Col14a1+}$, fibroblasts$^{Col13a1+}$, smooth muscle cells (SMC), endothelial, neutrophil, monocyte^{CD14+}, monocyte^{CD14-}, alveolar macrophages, circulatory proliferating macrophages, interstitial macrophages, plasma cells, B cells, natural killer cells (NK), and T cells. Each cluster included cells from the control and SiNPs-exposure groups (Figure 2C). Next, we divided all cells into four subgroups, immune (88.04% vs 92.19%, Control vs SiNPs), epithelial (2.28% vs 2.13%), endothelial (4.58% vs 2.03%), and mesenchymal cells (5.10% vs 3.65%), and calculated their proportion (Figure 2F).

3.3. Cell Communication Analysis in Lung Damage Caused by SiNPs

Cell-to-cell communication plays a crucial role in lung injury, coordinating the actions of various cells and performing as a whole. Here, we generated network-level maps of cell−cell signaling across 16 clusters, including epithelial, endothelial, mesenchymal, and immune cell types based on computational assessments of predicted ligand−receptor interactions (Figure 3A). Further, we evaluated the intercellular interactions among four subgroups, i.e., immune, epithelial, endothelial, and mesenchymal cells (Figure 3B and C). The enhanced intercellular interactions were shown in epithelial targeting mesenchymal or immune cells. This phenomenon may be attributed to the increased exosome secretion in epithelial

https://doi.org/10.1021/envhealth.4c00052
Environ. Health 2024, 2, 786−801

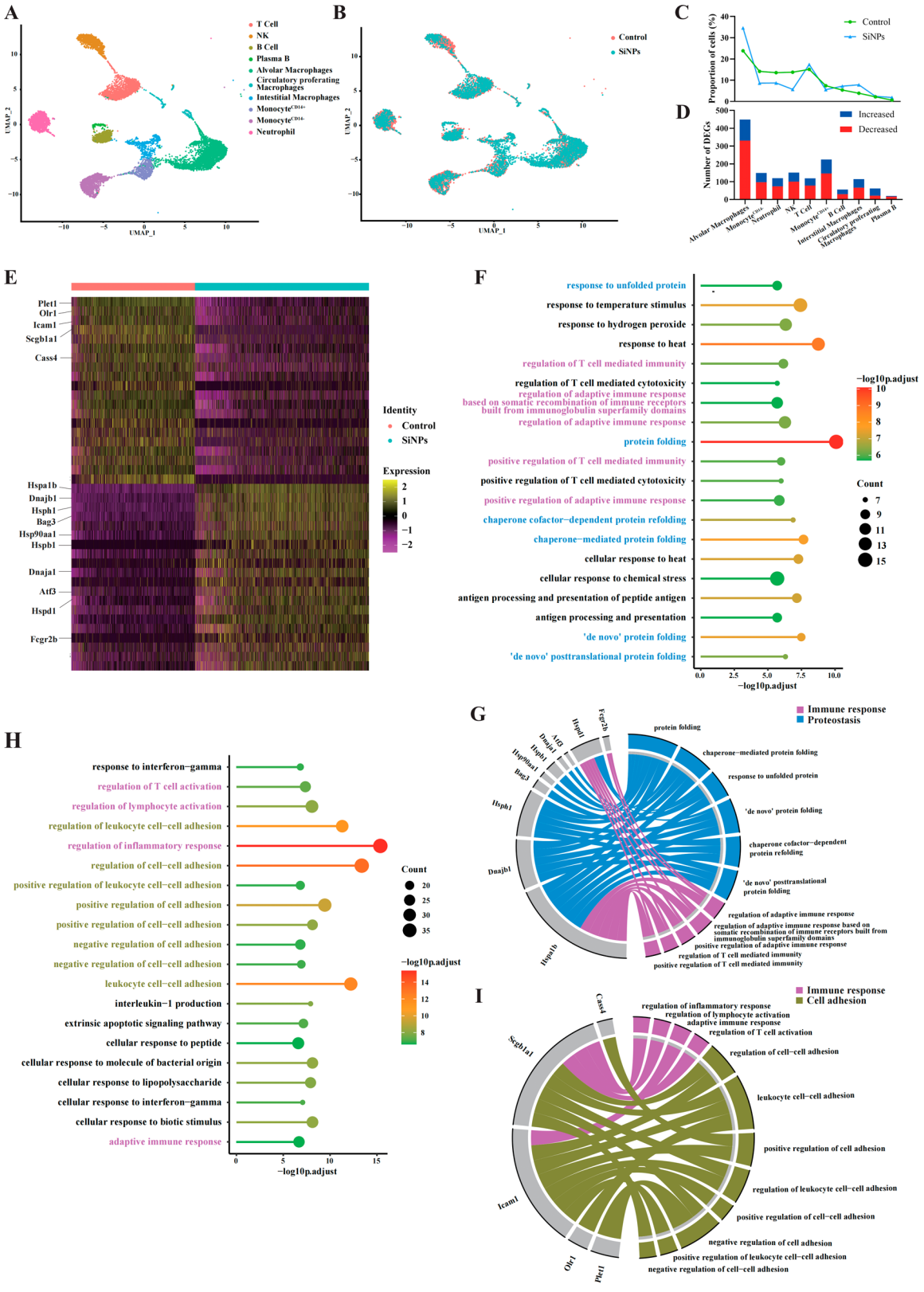

Figure 4. Immune subtype's transcriptome responses to SiNPs exposure. UMAP of immune cells from control and SiNPs exposure lungs are labeled by cell type (A) and exposure category (B). (C) Composition percentage of immune subtypes for each group. (D) The numbers of DEGs for each lung cell type in immune cells. Red indicates downregulated gene numbers, while blue indicates upregulated gene numbers. (E) Heatmap analysis of the DEGs reflected the perturbations of SiNPs on gene expressions in alveolar macrophage cells. GO analysis of DEGs in SiNPs-exposed rat lung with up- (F) and downregulation (H) in alveolar macrophage cells. Chordal graphs connecting the SiNPs-associated GO terms and the crucial up- (G) and downregulated (I) genes.

https://doi.org/10.1021/envhealth.4c00052
Environ. Health 2024, 2, 786−801

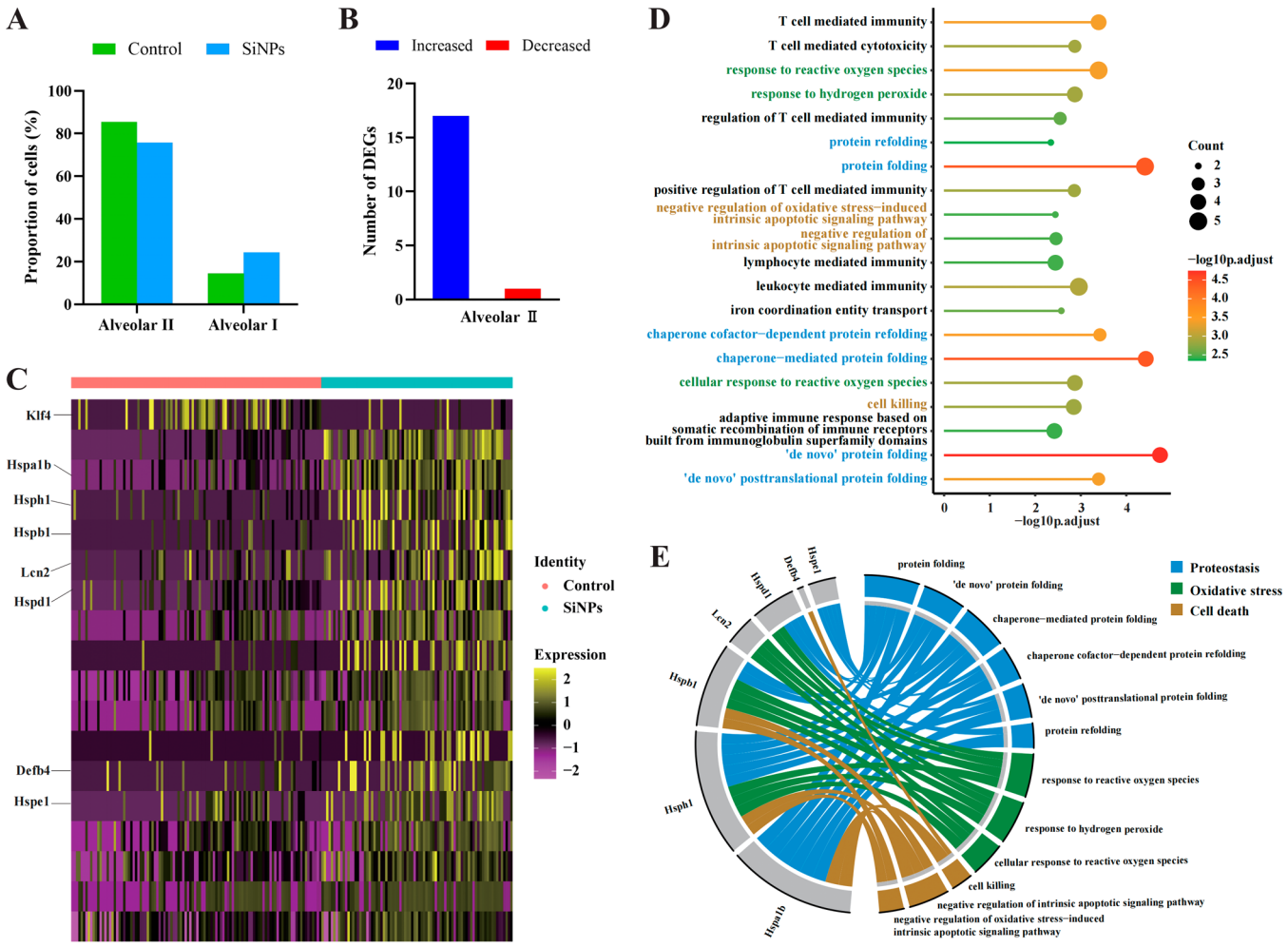

Figure 5. Epithelial subtype's transcriptome responses to SiNPs exposure. (A) Composition percentage of epithelial subtypes for each group. (B) The numbers of DEGs for each lung cell type in alveolar II cells. (C) Heatmap analysis of the DEGs presents the perturbations of SiNPs on gene expressions in alveolar II cells. (D) GO analysis of DEGs in SiNPs-exposed rat lung with upregulation in alveolar II cells and the chordal graphs (E) connecting the SiNPs-related GO terms and the crucial upregulated genes.

cells,[28] contributing to the activation of lung inflammation and fibrogenesis.[29−31] The receptor−ligand interactions among alveolar macrophages, alveolar II, and fibroblasts$^{Col14a1+}$ are present in Figure 3D. It illustrates that fibroblast$^{Col14a1+}$ can interact with alveolar macrophages and alveolar II cells mainly *via* COL1A1-CD44 and COL1A1-SDC4, ultimately leading to lung injury and collagen accumulation.

3.4. SiNPs Triggered Immune Response and Proteostatic Stress Response in Alveolar Macrophages

In light of their crucial role in the histopathology of lung interstitial injury, the transcriptional profiles of immune cell populations were assessed. In total, 9414 individual immune cells were captured, divided into 10 distinct clusters. All major immune cell types were identified, including neutrophil, monocyte^{CD14+}, monocyte^{CD14-}, alveolar macrophages, circulatory proliferating macrophages, interstitial macrophages, plasma cells, B cells, natural killer cells (NK), and T cells (Figure 4A−B). Although all of these major cell types were present in both the control and SiNPs-treated lungs, the cell proportion was varied (Figure 4C). The proportions of alveolar macrophages and interstitial macrophages were greatly increased after SiNPs exposure in comparison to the control group, while that of NK, neutrophil, and monocyte^{CD14-} cells was reduced. According to the number of DEGs per cluster in the immune cell population (Figure 4D), the transcriptome of alveolar macrophages (including 449 DEGs) was the most affected by SiNPs. Herein, we focused on the DEGs on the alveolar macrophages cluster between the control and SiNPs group (Figure 4E). The following GO enrichment analysis clarified that DEGs ($|FC| > 2$, adjusted $p < 0.05$) attributed to SiNPs exposure were tightly related to immune response, proteostatic stress response (proteostasis), and cell adhesion (Figure 4F−I). The significant pathways identified by upregulated DEGs focused on immune response, protein folding, and cell stress (Figure 4F). Then the GO chord was used to connect the essential upregulated genes and biological processes (Figure 4G). Protein homeostasis was essential for the normal physiological function of alveolar macrophages, with 9 of 10 vital genes involved. Besides, two of the nine enriched genes overlapped in alveolar macrophage-mediated immune response elicited by SiNPs (Figure 4G), which were Hspa1b and Hspd1. It hints at a possible link between the immune response activation and proteostatic stress response induced by SiNPs. Comparatively, downregulated DEGs were mainly involved in the regulation of cell adhesion and immune response (Figure 4H−I). Taken together, we speculated SiNPs

https://doi.org/10.1021/envhealth.4c00052
Environ. Health 2024, 2, 786−801

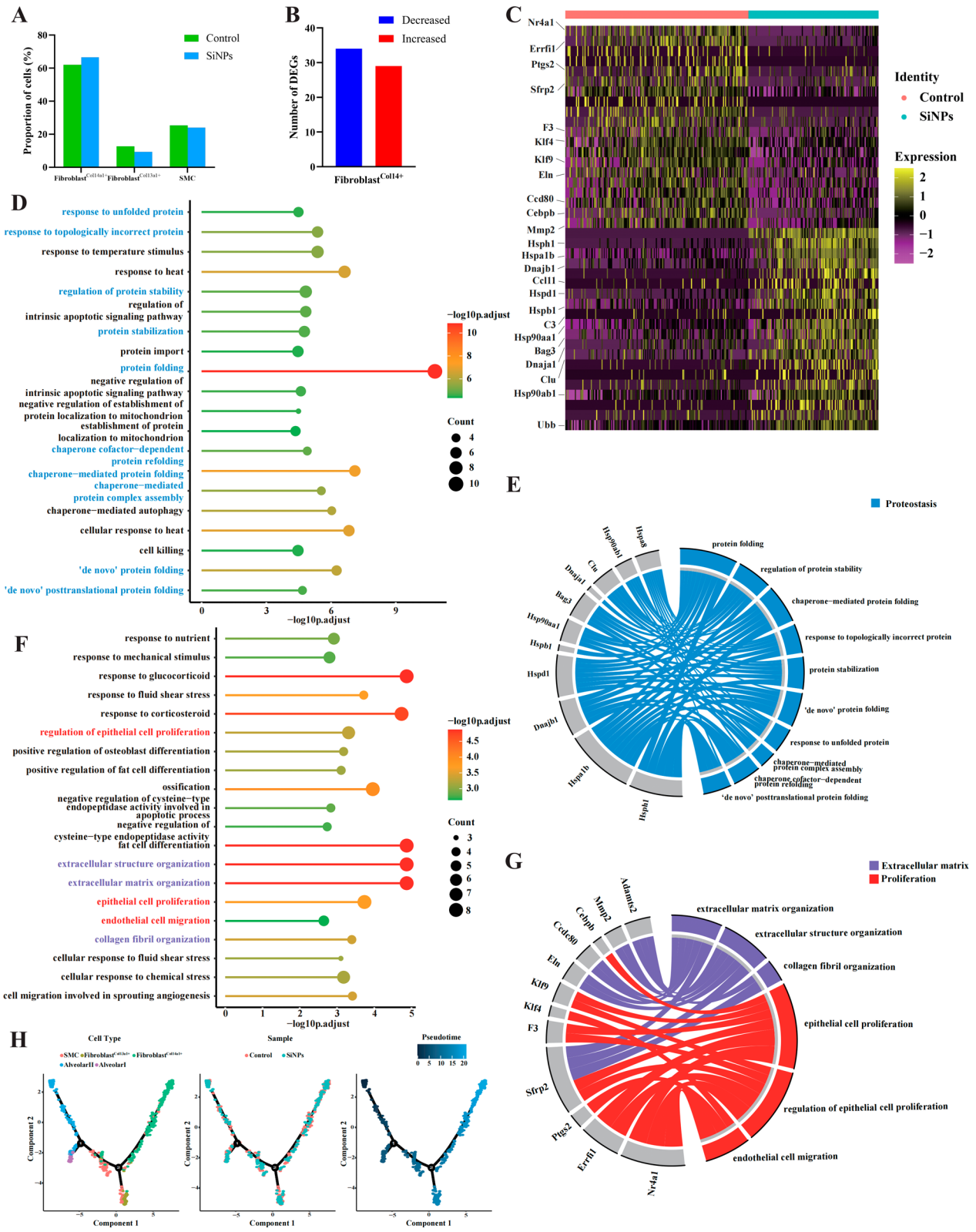

Figure 6. Mesenchymal subtype's transcriptome responses to SiNPs exposure. (A) The proportion of mesenchymal subtypes for each group. (B) The DEGs numbers for each lung cell type in fibroblast$^{Col14a1+}$ cells. (C) Heatmap analysis of the DEGs revealed the perturbations of SiNPs on gene expressions in fibroblast$^{Col14a1+}$ cells. GO analysis of DEGs in SiNPs-exposed rat lung with up- (D) and downregulation (F) in fibroblast$^{Col14a1+}$ cells. Chordal graphs connecting the SiNPs-associated GO terms and the crucial up- (E) and downregulated (G) genes. (H) Pseudotime trajectory of lung single cell, including epithelial and fibroblast transcriptomes colored by cell type, sample, and pseudotime, respectively.

primarily triggered immune response, proteostatic stress response, and cell adhesion in the alveolar macrophages to contribute to the pathogenesis of pulmonary inflammation and resultant lung interstitial injury.

https://doi.org/10.1021/envhealth.4c00052
Environ. Health 2024, 2, 786−801

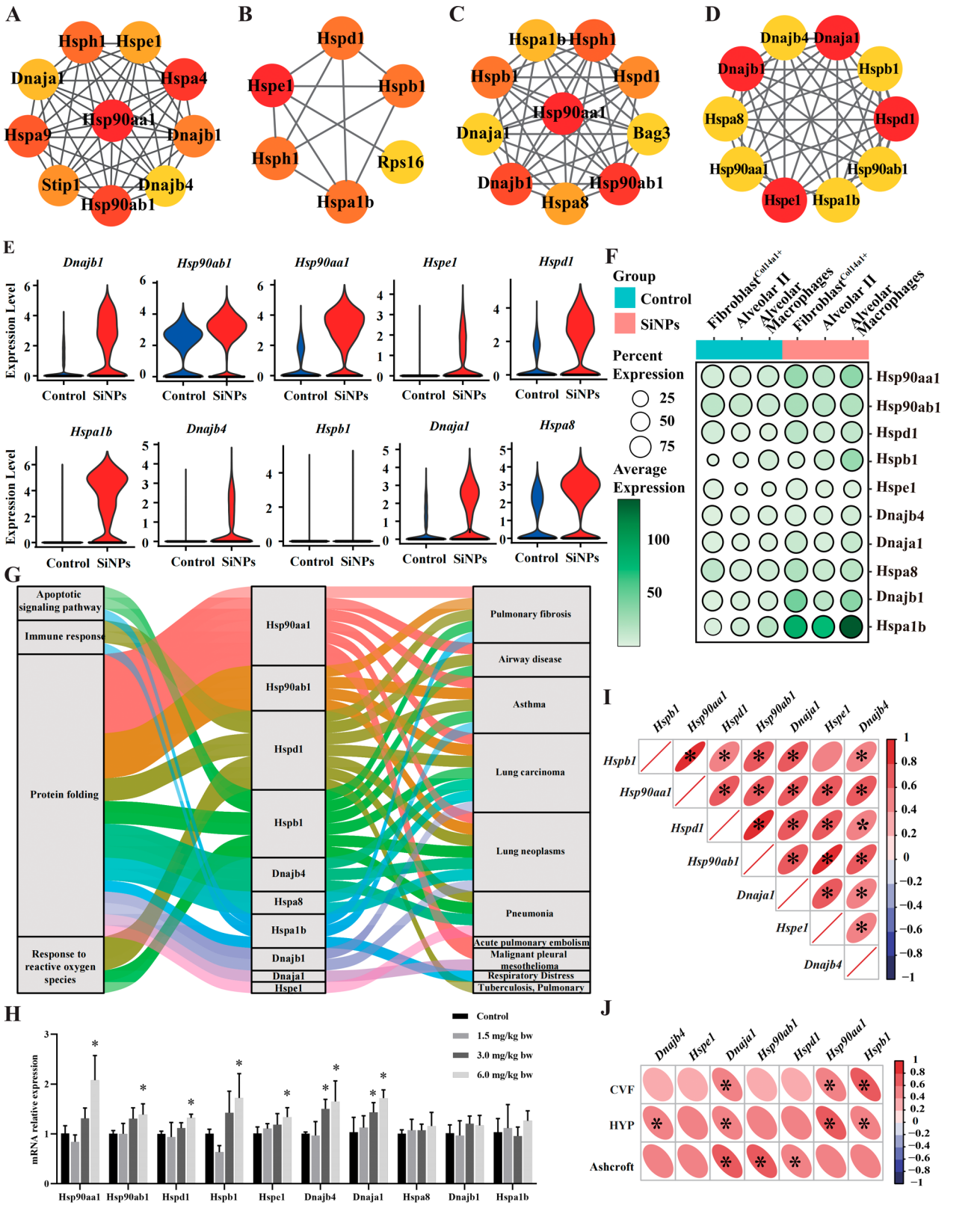

Figure 7. SiNPs triggered heat shock stress and proteostasis disorder. The top genes are ranked by the MCC method in alveolar macrophage cells (A), alveolar II cells (B), and fibroblast$^{Col14a1+}$ cells (C). (D) The Hsps genes involved in lung-related disease. The violin plots (E) were used to show their expressions in the whole lung, and the dot plot (F) was applied to show their expressions in each cell cluster. (G) Hsps genes involved in immune response, protein folding, apoptotic signaling pathway, and response to ROS participated in pulmonary diseases. (H) qRT-PCR verified SiNPs activated the expressions of *Hspb1*, *Hsp90aa1*, *Hspd1*, *Hsp90ab1*, *Dnajb1*, and *Dnaja1* (n = 4). The correlation between Hsps genes (I) and between Hsps genes and lung injury-related indicators (J) was calculated. The red color indicates a positive correlation. *p < 0.05, compared with control.

https://doi.org/10.1021/envhealth.4c00052
Environ. Health 2024, 2, 786−801

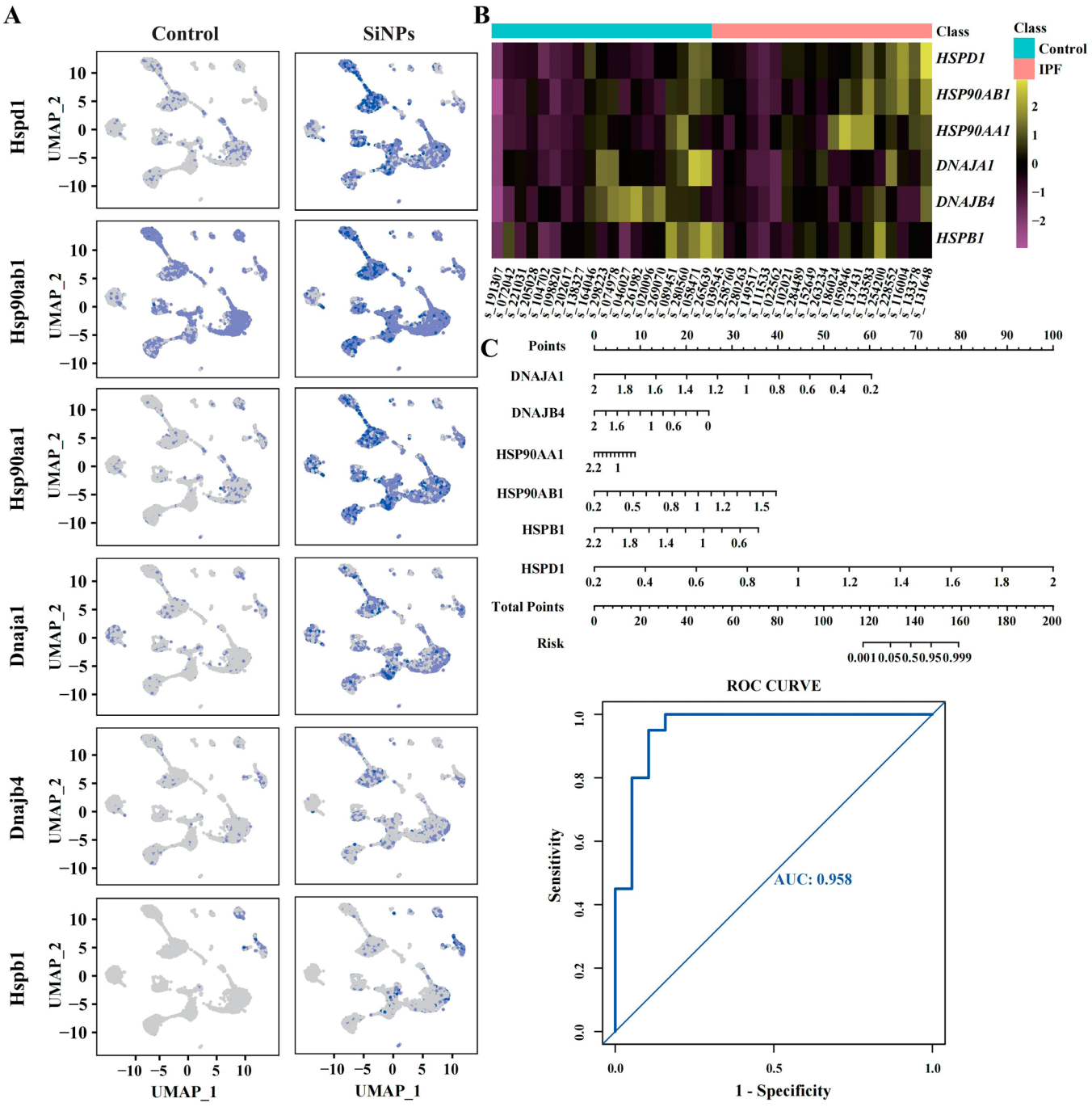

Figure 8. Hsps gene expressions in the lung. (A) The UMAP reflected the Hsps gene expressions in each cell cluster. (B) Heatmap analysis of the Hsps genes in the IPF patients. (C) A nomogram for predicting the risk of IPF was conducted and verified by AUC.

3.5. SiNPs Disturbed Proteostatic Stress Response, Oxidative Stress, and Cell Death in Alveolar Epithelial Cells

It is generally accepted that lung epithelial cells had an important role in maintaining lung homeostasis, function, and injury repair. Herein, we captured all alveolar epithelial cell populations in control and SiNPs exposure rats. As shown in Figure 5A, more than 80% of captured alveolar epithelial cells were type II in the control lung, and a declined proportion of alveolar II cells was noticed upon SiNPs exposure. That may be explained by the differentiation of alveolar II into alveolar I in response to the damage on pulmonary alveolar epithelial cells by SiNPs.[32−34] DEGs were detected in alveolar II cells upon SiNPs exposure but not in alveolar I cells owing to its small quantity. SiNPs exposure distinctly varied 18 genes' expression in alveolar II cells, including 17 upregulated and 1 downregulated genes (Figure 5B−C). The following GO annotation analysis (Figure 5D−E) showed the three major biological processes initiated by SiNPs were proteostasis, oxidative stress, and cell death. Figure 5E represents the correlation between key upregulated genes (|FC| > 2, adjusted $p < 0.05$) and biological processes. According to the GO chord graph, five pivotal genes were all involved in the protein folding and protein refolding process, revealing proteostasis as the most affected bioprocess in alveolar epithelial cells after SiNPs exposure. Besides, proteostasis may be associated with the

https://doi.org/10.1021/envhealth.4c00052
Environ. Health 2024, 2, 786−801

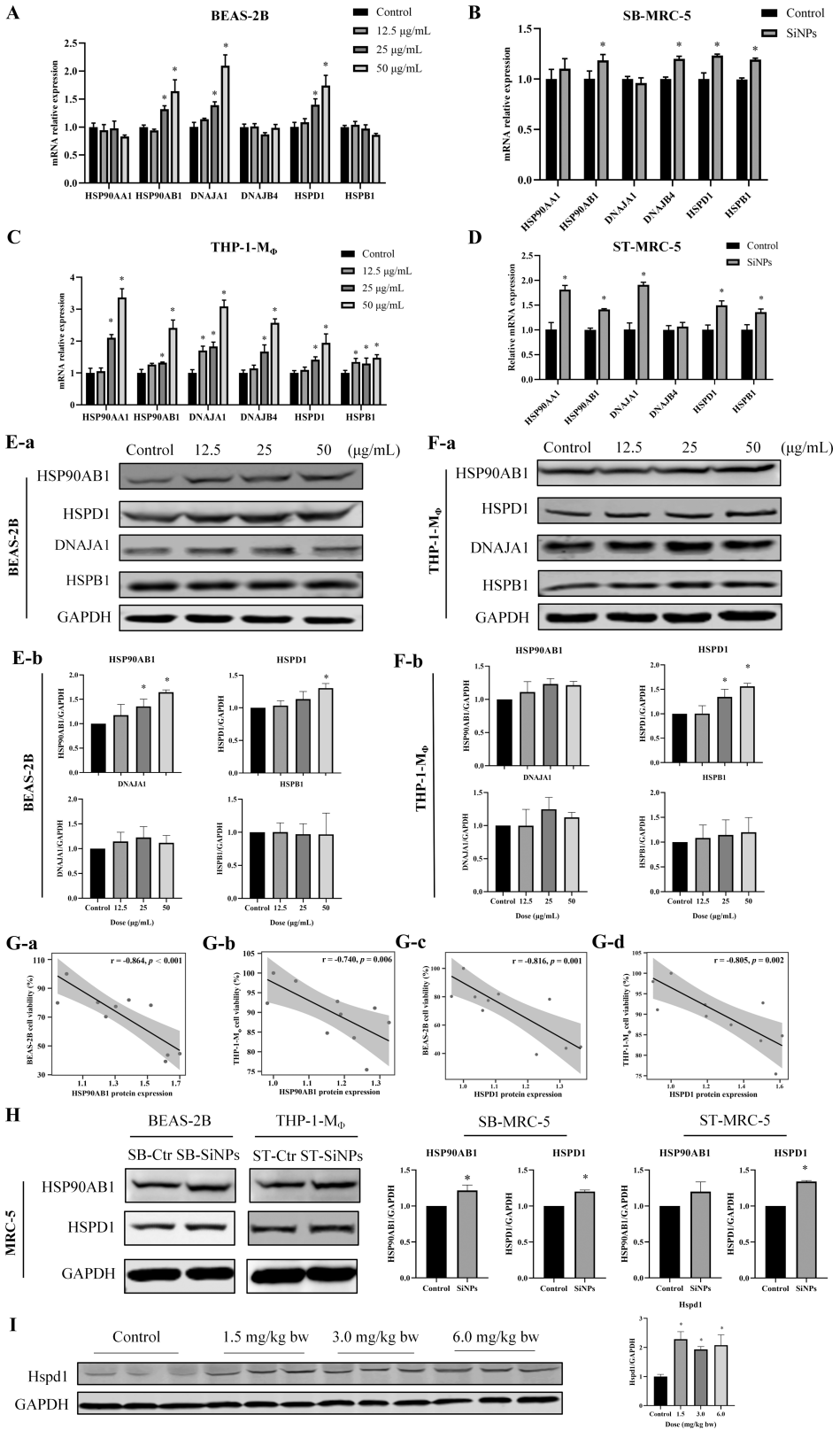

Figure 9. Hsps genes expressions *in vitro* and *in vivo*. qRT-PCR verified the expressions of candidate Hsps genes in BEAS-2B epithelial cells (A) and its supernatants stimulated MRC-5 fibroblasts (B) and THP-1-M_Φ (C) and its supernatants stimulated MRC-5 fibroblasts (D). Then, Western blot verified the expressions of filtered Hsps, HSP90AB1, HSPD1, DNAJA1, and HSPB1 in BEAS-2B cells (E) and its supernatants stimulated MRC-5 cells (H, left) and THP-1-M_Φ (F) and its supernatants stimulated MRC-5 cells (H, right). Correlation analysis showed the negative regulatory relationships between SiNPs-induced HSP90AB1/HSPD1 expression and cellular viability in either BEAS-2B (Figure 9G-a,c) or THP-1-M_Φ cells (Figure 9G-b,d). Consistently, Hspd1 was also upregulated in the lung tissue (I). $n = 3$, $^*p < 0.05$, compared with control or SB-Ctr/ST-Ctr.

https://doi.org/10.1021/envhealth.4c00052
Environ. Health 2024, 2, 786−801

activation of oxidative stress and cell death, since three of the five enriched genes overlapped in oxidative stress and three of the five genes in cell death. These data highlighted that SiNPs could disturb the proteostatic stress response and activate oxidative stress and cell death in lung epithelial cells, contributing to the onset and progression of pulmonary interstitial injury.

3.6. SiNPs Induced Proteostatic Stress Response, Extracellular Matrix Deposition, and Cell Proliferation in Lung Fibroblasts

As shown in Figure 6A, most of the identified cells in lung interstitium were fibroblasts, especially the fibroblasts with positive expression of Col14a1 (fibroblast$^{Col14a1+}$). The cell proportion in each cluster was similar between the control and SiNPs group. Sixty-three DEGs were assessed in fibroblast$^{Col14a1+}$, of which 34 were significantly upregulated and 29 were downregulated (Figure 6B,C). GO analysis revealed the key biological processes in fibroblasts owing to SiNPs exposure, that is, proteostatic stress response attributed to the upregulated DEGs (Figure 6D), while extracellular matrix (ECM) organization and cell proliferation were responsible for the downregulated DEGs (Figure 6F). As depicted in Figure 6E,G, GO chord disclosed the correlation between crucial up- and downregulated genes ($|FC| > 2$, adjusted $p < 0.05$) and corresponding biological process. Interestingly, we observed that Klf4 was downregulated in both alveolar II cells and fibroblast$^{Col14a1+}$ and was involved in the biological process of epithelial cell proliferation (Figure 6G). Further, the cell trajectory of epithelial and interstitial cells in the lungs was conducted (Figure 6H). Alveolar epithelial cells and lung interstitial cells were in separate branches of the trajectory, an indication of their distinct differentiation states. SMC cells were between the epithelial cells and fibroblast branches, implying the intermediate differentiation state. The fibroblast activation was observed in the final stage. In brief, the lung insult by SiNPs may result in abnormal crosstalk between epithelial cells and fibroblasts and even the occurrence of epithelial−mesenchymal transition (EMT).

3.7. Perturbed Heat Shock Stress May Contribute to the Pulmonary Injury Caused by SiNPs

According to the gene interaction analysis of all DEGs in alveolar macrophages cells (Figure 7A), alveolar II cells (Figure 7B), and fibroblast$^{Col14a1+}$ cells (Figure 7C) *via* the MCC method, we were surprised to discover that the genes of the heat shock protein (Hsps) family were dominant in all these three types of cells. Based on the interaction network analysis, gene expression, and disease-targeting prediction (Figure 7D), 10 out of the 13 Hsps family genes were thought to be involved in lung injury and pulmonary diseases. Meanwhile, the expressions of these genes in alveolar II cells, macrophage, fibroblasts, and the whole lung tissue are shown in Figure 7E−F. As manifested in Figure 7G, the alterations of Hsps family genes may affect the onset and development of SiNPs-elicited lung disease through apoptotic signaling pathway, immune response, protein folding, and response to reactive oxygen species (ROS). The verification by qRT-PCR (Figure 7H) showed increased transcription of seven Hsps in lung tissue upon SiNPs stimulation, which were closely interconnected (Figure 7I). Moreover, the correlations analysis (Figure 7J) implied the six candidate Hsps family genes (*Hsp90ab1*, *Hsp90aa1*, *Hspb1*, *Dnaja1*, *Hspd1*, *Dnajb4*) as the potential mediators in SiNPs-elicited lung impairments.

3.8. Hspd1 May Play a Crucial Role in the Pulmonary Interstitial Injury

We have discerned the ubiquitous expression of six candidate genes across a spectrum of pulmonary cell types, implying their potential participation in the regulation of diverse cells throughout the stages of disease onset and progression (Figure 8A). Based on the GEO database, the gene expression of related Hsps was manifested in heatmap (Figure 8B). Then, we constructed a nomogram for pulmonary interstitial according to the filtered variables (Figure 8C), and AUC was more than 0.9, indicating favorable discrimination by the nomogram. Of note, *HSPD1* (coefficient = 18.4405, $p < 0.05$; Table S2) may be a crucial candidate gene to indicate pulmonary interstitial injury. A consistent result was found in the nomogram for pulmonary parenchyma (Figure S2), based on alveolar II data (*Hspd1* coefficient = 0.5746, $p < 0.05$; Table S3). To confirm our findings, we measured the expressions of *Hsp90ab1*, *Hsp90aa1*, *Hspb1*, *Dnaja1*, *Hspd1*, and *Dnajb4* in the different models *in vitro* by qRT-PCR and Western blot (Figure 9A−H). Upon the exposure to SiNPs, HSP90AB1 and HSPD1 expressions in lung epithelial (BEAS-2B) and macrophages (THP-1-M_Φ) were remarkably upregulated, which were correlated to SiNPs-elicited cell viability decline (Figure 9G). In particular, HSPD1 was greatly upregulated in fibroblasts (Figure 9H). In line with the *in vitro* data, the enhanced expression of Hspd1 was also validated in the SiNPs-treated lung tissue (Figure 9I). Taken together, our data hinted that Hspd1 may be an essential indicator in SiNPs-caused lung interstitial injury.

4. DISCUSSION

Considering the applicability and accessibility of SiNPs, the toxicity of SiNPs should be exactly estimated. A large number of studies have confirmed that SiNPs could enhance lung permeability,[35] exacerbate pulmonary inflammation[36] and fibrosis progression,[33,37] and even present the carcinogenic potential of lung cancer.[16] Likewise, we noticed lung interstitial injury in rat lung tissues exposed to SiNPs, as manifested by alveolar septa thickening (Figure 1A) and collagen hyperplasia (Figure 1B−C). Still, the molecular mechanisms and intercellular crosstalk regarding SiNPs-elicited respiratory diseases have not been comprehensively revealed. Diverse and heterogeneous biological processes and various cell types were involved in the pathogenesis of pulmonary impairments. For these issues, we disclosed the cell-specific response at the single-cell level in the rat lung owing to SiNPs exposure. Based on the biological process in GO and KEGG analysis (Figures 4−6), the disordered effects among the various pulmonary cells were principally linked with proteostasis, accompanied by the immune response in macrophages (Figure 4), oxidative stress, and cell death process in epithelial cells (Figure 5) and ECM organization and proliferation in fibroblasts (Figure 6).

The major cell types responsible for pulmonary diseases are macrophages, alveolar epithelial cells, and fibroblasts. Dysregulation of these cells exerts their profibrotic roles *via* affecting pathological mechanisms such as immune response, oxidative stress, cell proliferation, and apoptosis, which ultimately results in the development of pulmonary impairments. The activated alveolar macrophage was the dominant cell type in the rat lung, as identified in our scRNA-seq analysis. In accordance with experimental evidence, macrophages were considered as dominant internalized cells upon NPs stimuli in the lung[38]

https://doi.org/10.1021/envhealth.4c00052
Environ. Health 2024, 2, 786−801

and triggered immune response, exaggerated cascades of inflammatory response to precede lung inflammation, or even profibrotic development.[39,40] Epithelial remodeling was another important feature of pulmonary toxicity.[41] Concertedly, we previously revealed that SiNPs exposure could trigger oxidative stress, mitochondrial dysfunction, and ultimate irreversible cell death *via* apoptosis in lung epithelial cells.[15,42] Plenty of evidence has confirmed that the insult to alveolar epithelial cell integrity was in a central stage in disease susceptibility and initiation and/or progression of a wide host of lung diseases, especially in lung fibrosis.[43] In response to injured or stimulated lung epithelial cells by inhalants, interstitial repair *via* fibroblasts ensued, but its abnormal activation, proliferation, and excessive ECM deposition would drive the fibrosis occurrence and progression.[44,45] Of note, the interaction between epithelial cells and fibroblasts was well explained in the cell trajectory analysis (Figure 6H). The myofibroblasts in the lungs could be derived from EMT apart from the activation of resident fibroblasts. For another, SiNPs triggered heat shock response,[46] further affecting the proliferation and death of fibroblasts (Figure 6E and G).[47] Also, the activation of macrophage-mediated inflammatory response by SiNPs may promote the proliferation and differentiation of fibroblasts.[47] Collectively, all these cell-specific responses triggered by SiNPs and intercellular crosstalk in the lungs together constituted the pathogenesis of lung injury.

Cellular integrity depends on the correct protein folding of its protein components to maintain the specialized functions, support normal physiology, and protect humans from disease pathology. Interestingly, the dysregulated proteostasis was noticed in macrophages, alveolar epithelial cells, and also fibroblasts, which in particular served as the most influenced biological processes upon SiNPs stimuli. According to the literature, proteostasis perturbations have been identified in a series of pulmonary disorders.[48,49] Disturbances in cellular proteostasis can be harmful to the cell. An accumulation of evidence indicated that failing proteostasis may activate inflammatory responses.[50] The consequent release of proinflammatory mediators and excessive inflammation may contribute to dysfunctional proteostasis.[51,52] Likewise, Shin *et al.*[53] reported that altered proteostasis could result in inflammasome activation in macrophages. Even more, Watanabe *et al.*[54] concluded that ISRIB (an inhibitor of integrated stress response) promoted epithelial differentiation by resetting proteostasis and restoring protein translation to alleviate epithelial injury-mediated pulmonary fibroplasia. Besides, the activation of oxidative stress through ROS accumulation, a well-known crucial player in the adverse effects elicited by SiNPs, may lead to proteostasis disruption in the lungs.[55] Thereby, further clarification of the individual steps of proteostasis and inflammation, epithelial cell death and fibroblast-mediated ECM deposition, especially in humans, will offer a better apprehension of the cellular processes and open a window/path for the development of new intervention strategies for pulmonary injury elicited by SiNPs.

Hsps genes were known to participate in the protein quality control by promoting accurate folding of newly synthesized proteins and refolding of denatured proteins under a vast range of cellular stressor conditions.[56] Accumulative evidence has illustrated some specific Hsps may be the novel targets of viral lung diseases, fibrotic interstitial lung diseases, COPD, and lung cancer.[57−60] The dominant types of Hsps consist of five primary and highly conserved families, which are small heat shock proteins (sHsps), Hsp60s, Hsp70s, Hsp90s, and Hsp100s.[61] Our data suggested that SiNPs triggered Hsps stress, as evidenced by the upregulated transcription of Hspb1 (also known as Hsp27), Dnaja1 (a class I member of Hsp40), Dnajb1 (a class II member of Hsp40), Hspd1(also known as Hsp60), Hsp90aa1, and Hsp90ab1 (Figure 7). That may affect protein folding, apoptotic signaling pathway, immune response, and response to ROS, ultimately leading to lung diseases (Figure 7). It was worthy to note a consistent alteration in the expressions of Hsp27, Hsp40, Hsp60, and Hsp90 when cells were stimulated.[62] In particular, the validation of Hsps on SiNPs-elicited pulmonary toxicity using a set of *in vitro* models revealed that among these candidate Hsps, Hspd1 (Hsp60) showed more pronounced differences in lung cells or tissues upon the exposure to SiNPs (Figure 9). These data hinted at Hsps interventions, especially on Hspd1, probably as a potential target for therapeutic intervention to SiNPs-elicited lung impairments.

As the most abundant member of the sHsps, Hspb1 maintains denatured proteins in a fold-competent state, resulting in stress resistance.[63] The inhibition of Hspb1 by J2 (an inhibitor of Hspb1) has been pointed out to significantly attenuate inflammation and collagen accumulation in lung tissue.[64] Also, Hsp27 was reported to participate in the EMT process through activating the IkBα-NFκB pathway.[65] Both Dnaja1 and Dnajb1 bound to unfolded proteins to prevent their degradation[66] and were incorporated into stress granules.[67] According to the literature, Dnajb1 caused β-catenin and its phosphorylation at PKA phosphorylation site S675,[68] resulting in the induction of inflammation and fibrosis further. In contrast, Hsp40 could activate ATPase of Hsp70[69] and may serve as a potential therapeutic target to lessen lung damage.[70]

Hsp60 is a chaperone protein that normally acts within mitochondria to maintain protein homeostasis,[71] including protein folding, unfolding, and disaggregation.[72] Hsp60 has been reported to participate in the pathogenesis of inflammatory diseases through promoting higher levels of transforming growth factor (TGF-β) and interleukin-8 (IL-8) release.[73,74] When compared to healthy people, a remarkably high level of Hsp60 was present in patients with acute exacerbation of COPD.[75,76] Meanwhile, Hsp60 plays a crucial role as a node in intracellular molecular networks and a linking molecule in intercellular immune networks.[77] Evidence has illustrated that Hsp60 released from recurrently infected epithelial cells and macrophages caused prolonged antigenic stimulation so as to amplify chronic inflammation,[78] ultimately resulting in pathological tissue damage. Besides, as a critical regulator of proteostasis, Hsp90 has become a potential therapeutic target for diseases associated with protein misfolding.[79] The inhibitors of Hsp90 (AUY-922[80] and 17-AGG8[81]) have been confirmed to decrease the overexpression of collagen and ECM proteins and thereby to suppress lung fibrosis. Certainly, limited reports have documented the role of Hsps in the nanoparticles-elicited pulmonary toxicity. Hence, the underlying impact and potential mechanisms still remain issues that need to be explored.

5. CONCLUSION

The findings of our study first illuminated the pulmonary toxicity of SiNPs in Wistar rats from a cell-specific responses perspective. SiNPs disturbed proteostasis, and induced the

https://doi.org/10.1021/envhealth.4c00052
Environ. Health 2024, 2, 786−801

immune response in macrophages, oxidative stress and cell death in epithelial cells, and proliferation and ECM changes in fibroblasts, contributing to the pulmonary fibrotic effect. Also, we highlighted the Hsps through interfering proteostasis, especially Hspd1, as an underlying mediator to SiNPs-caused pulmonary interstitial disease. Certainly, more work was urgently needed to illuminate the mode of action and mechanisms of Hsps to participate in the fibrosis interstitial injury upon SiNPs stimuli. All in all, this study presented a comprehensive understanding of cellular-specific response in SiNPs-driven lung impairments and also provided novel insights into further mechanistic investigations and explorations for preventive and treatment interventions.

■ ASSOCIATED CONTENT

Supporting Information

The Supporting Information is available free of charge at https://pubs.acs.org/doi/10.1021/envhealth.4c00052.

Additional experimental details, materials, and methods, including cell viability, primer sequences, and nomogram data (PDF)

■ AUTHOR INFORMATION

Corresponding Authors

Yanbo Li − *Beijing Key Laboratory of Environmental Toxicology, Capital Medical University, Beijing 100069, China; Department of Toxicology and Sanitary Chemistry, School of Public Health, Capital Medical University, Beijing 100069, China;* orcid.org/0000-0001-5414-0736; Email: ybli@ccmu.edu.cn

Caixia Guo − *Department of Occupational Health and Environmental Health, School of Public Health and Beijing Key Laboratory of Environmental Toxicology, Capital Medical University, Beijing 100069, China*; Email: guocx@ccmu.edu.cn

Authors

Yan Li − *Department of Occupational Health and Environmental Health, School of Public Health and Beijing Key Laboratory of Environmental Toxicology, Capital Medical University, Beijing 100069, China*

Qing Yao − *Beijing Key Laboratory of Environmental Toxicology, Capital Medical University, Beijing 100069, China; Department of Toxicology and Sanitary Chemistry, School of Public Health, Capital Medical University, Beijing 100069, China*

Hailin Xu − *Beijing Key Laboratory of Environmental Toxicology, Capital Medical University, Beijing 100069, China; Department of Toxicology and Sanitary Chemistry, School of Public Health, Capital Medical University, Beijing 100069, China*

Jiaze Ren − *Department of Occupational Health and Environmental Health, School of Public Health and Beijing Key Laboratory of Environmental Toxicology, Capital Medical University, Beijing 100069, China*

Yurou Zhu − *Beijing Key Laboratory of Environmental Toxicology, Capital Medical University, Beijing 100069, China; Department of Toxicology and Sanitary Chemistry, School of Public Health, Capital Medical University, Beijing 100069, China*

Complete contact information is available at: https://pubs.acs.org/10.1021/envhealth.4c00052

Notes

The authors declare no competing financial interest.

■ ACKNOWLEDGMENTS

This work has been financially supported by the National Natural Science Foundation of China (82273658, 82173551) and Special Funds for the Construction of High-level Public Health Technical Talents (xuekegugan-01-048).

■ REFERENCES

(1) Mebert, A. M.; Baglole, C. J.; Desimone, M. F.; Maysinger, D. Nanoengineered silica: Properties, applications and toxicity. *Food Chem. Toxicol.* **2017**, *109*, 753−770.

(2) Al-Kattan, A.; Wichser, A.; Vonbank, R.; Brunner, S.; Ulrich, A.; Zuin, S.; Arroyo, Y.; Golanski, L.; Nowack, B. Characterization of materials released into water from paint containing nano-SiO2. *Chemosphere* **2015**, *119*, 1314−1321.

(3) OECD. *Series on the Safety of Manufactured Nanomaterials No. 90. Physical-Chemical Decision Framework to Inform Decisions for Risk Assessment of Manufactured Nanomaterials Organisation for Economic Co-operation and Development*. 2019. http://www.oecd.org/officialdocuments/publicdisplaydocumentpdf/?cote=env/jm/mono(2019)12&doclanguage=en.

(4) Guo, C.; Liu, Y.; Li, Y. Adverse effects of amorphous silica nanoparticles: Focus on human cardiovascular health. *J. Hazard Mater.* **2021**, *406*, 124626.

(5) Zhao, X.; Wu, Y.; Li, J.; et al. JNK activation-mediated nuclear SIRT1 protein suppression contributes to silica nanoparticle-induced pulmonary damage via p53 acetylation and cytoplasmic localisation. *Toxicology* **2019**, *423*, 42−53.

(6) Zhang, L.; Wei, J.; Duan, J.; Guo, C.; Zhang, J.; Ren, L.; Liu, J.; Li, Y.; Sun, Z.; Zhou, X. Silica nanoparticles exacerbates reproductive toxicity development in high-fat diet-treated Wistar rats. *J. Hazard Mater.* **2020**, *384*, 121361.

(7) Abulikemu, A.; Zhao, X.; Xu, H.; Li, Y.; Ma, R.; Yao, Q.; Wang, J.; Sun, Z.; Li, Y.; Guo, C. Silica nanoparticles aggravated the metabolic associated fatty liver disease through disturbed amino acid and lipid metabolisms-mediated oxidative stress. *Redox Biol.* **2023**, *59*, 102569.

(8) Li, X.; Xu, H.; Zhao, X.; Li, Y.; Lv, S.; Zhou, W.; Wang, J.; Sun, Z.; Li, Y.; Guo, C. Ferroptosis contributing to cardiomyocyte injury induced by silica nanoparticles via miR-125b-2−3p/HO-1 signaling. *Part. Fibre Toxicol.* **2024**, *21*, 17.

(9) Diao, J.; Xia, Y.; Jiang, X.; et al. Silicon dioxide nanoparticles induced neurobehavioral impairments by disrupting microbiota-gut-brain axis. *J. Nanobiotechnol.* **2021**, *19*, 174.

(10) Setyawati, M. I.; Singh, D.; Krishnan, S. P. R.; et al. Occupational Inhalation Exposures to Nanoparticles at Six Singapore Printing Centers. *Environ. Sci. Technol.* **2020**, *54*, 2389−2400.

(11) Debia, M.; Carpentier, M.; L'Esperance, G. Characterization of Occupational Exposures to Engineered Nanoparticles During the Finishing Process of a Hardwood Floor Manufacturing Plant. *Ann. Work Expo Health* **2021**, *65*, 868−873.

(12) Li, Y.; Xu, H.; Wang, Y.; Zhu, Y.; Xu, K.; Yang, Z.; Li, Y.; Guo, C. Epithelium-derived exosomes promote silica nanoparticles-induced pulmonary fibroblast activation and collagen deposition via modulating fibrotic signaling pathways and their epigenetic regulations. *Journal of Nanobiotechnology* **2024**, *22*, 331.

(13) Marques Da Silva, V.; Benjdir, M.; Montagne, P.; Pairon, J.-C.; Lanone, S.; Andujar, P. Pulmonary Toxicity of Silica Linked to Its Micro- or Nanometric Particle Size and Crystal Structure: A Review. *Nanomaterials (Basel)* **2022**, *12*, 2392.

(14) Kolling, A.; Ernst, H.; Rittinghausen, S.; Heinrich, U. Relationship of pulmonary toxicity and carcinogenicity of fine and

ultrafine granular dusts in a rat bioassay. *Inhal. Toxicol.* **2011**, *23*, 544−554.
(15) Li, Y.; Zhu, Y.; Zhao, B.; Yao, Q.; Xu, H.; Lv, S.; Wang, J.; Sun, Z.; Li, Y.; Guo, C. Amorphous silica nanoparticles caused lung injury through the induction of epithelial apoptosis via ROS/Ca(2+)/DRP1-mediated mitochondrial fission signaling. *Nanotoxicology* **2022**, *16*, 713−732.
(16) Guo, C.; Wang, J.; Yang, M.; Li, Y.; Cui, S.; Zhou, X.; Li, Y.; Sun, Z. Amorphous silica nanoparticles induce malignant transformation and tumorigenesis of human lung epithelial cells via P53 signaling. *Nanotoxicology* **2017**, *11*, 1176−1194.
(17) Park, H. J.; Sohn, J. H.; Kim, Y. J.; et al. Acute exposure to silica nanoparticles aggravate airway inflammation: different effects according to surface characteristics. *Exp Mol. Med.* **2015**, *47*, No. e173.
(18) Liao, H. Y.; Chung, Y. T.; Lai, C. H.; et al. Six-month follow-up study of health markers of nanomaterials among workers handling engineered nanomaterials. *Nanotoxicology* **2014**, *8*, 100−110.
(19) Ardlie, K. G.; et al. The Genotype-Tissue Expression (GTEx) pilot analysis: multitissue gene regulation in humans. *Science* **2015**, *348*, 648−660.
(20) Hedlund, E.; Deng, Q. Single-cell RNA sequencing: Technical advancements and biological applications. *Mol. Aspects Med.* **2018**, *59*, 36−46.
(21) Hwang, B.; Lee, J. H.; Bang, D. Single-cell RNA sequencing technologies and bioinformatics pipelines. *Exp Mol. Med.* **2018**, *50*, 1−14.
(22) Farber, D. L.; Sims, P. A. Dissecting lung development and fibrosis at single-cell resolution. *Genome Med.* **2019**, *11*, 33.
(23) Stark, R.; Grzelak, M.; Hadfield, J. RNA sequencing: the teenage years. *Nat. Rev. Genet* **2019**, *20*, 631−656.
(24) Franks, T. J.; Colby, T. V.; Travis, W. D.; et al. Resident cellular components of the human lung: current knowledge and goals for research on cell phenotyping and function. *Proc. Am. Thorac. Soc.* **2008**, *5*, 763−766.
(25) Travaglini, K. J.; Nabhan, A. N.; Penland, L.; et al. A molecular cell atlas of the human lung from single-cell RNA sequencing. *Nature* **2020**, *587*, 619−625.
(26) Chen, S.; Zhou, Y.; Chen, Y.; Gu, J. fastp: an ultra-fast all-in-one FASTQ preprocessor. *Bioinformatics* **2018**, *34*, i884−i890.
(27) Trapnell, C.; Cacchiarelli, D.; Grimsby, J.; et al. The dynamics and regulators of cell fate decisions are revealed by pseudotemporal ordering of single cells. *Nat. Biotechnol.* **2014**, *32*, 381−386.
(28) Kulshreshtha, A.; Ahmad, T.; Agrawal, A.; Ghosh, B. Proinflammatory role of epithelial cell-derived exosomes in allergic airway inflammation. *J. Allergy Clin Immunol* **2013**, *131*, 1194−1203.
(29) Gong, T.; Zhang, X.; Liu, X.; et al. Exosomal Tenascin-C primes macrophage pyroptosis amplifying aberrant inflammation during sepsis-induced acute lung injury. *Transl. Res.* **2024**, *270*, 66−80.
(30) Kadota, T.; Fujita, Y.; Araya, J.; et al. Human bronchial epithelial cell-derived extracellular vesicle therapy for pulmonary fibrosis via inhibition of TGF-β-WNT crosstalk. *J. Extracell. Vesicles* **2021**, *10*, No. e12124.
(31) Zhang, M.; Xue, X.; Lou, Z.; Lin, Y.; Li, Q.; Huang, C. Exosomes from senescent epithelial cells activate pulmonary fibroblasts via the miR-217−5p/Sirt1 axis in paraquat-induced pulmonary fibrosis. *J. Transl. Med.* **2024**, *22*, 310.
(32) Ruaro, B.; Salton, F.; Braga, L.; Wade, B.; Confalonieri, P.; Volpe, M. C.; Baratella, E.; Maiocchi, S.; Confalonieri, M. The History and Mystery of Alveolar Epithelial Type II Cells: Focus on Their Physiologic and Pathologic Role in Lung. *Int. J. Mol. Sci.* **2021**, *22*, 2566.
(33) Zhao, X.; Wei, S.; Li, Z.; Lin, C.; Zhu, Z.; Sun, D.; Bai, R.; Qian, J.; Gao, X.; Chen, G.; Xu, Z. Autophagic flux blockage in alveolar epithelial cells is essential in silica nanoparticle-induced pulmonary fibrosis. *Cell Death Dis.* **2019**, *10*, 127.
(34) Lin, Y.-J.; Yang, C.-C.; Lee, I-T.; Wu, W.-B.; Lin, C.-C.; Hsiao, L.-D.; Yang, C.-M. Reactive Oxygen Species-Dependent Activation of EGFR/Akt/p38 Mitogen-Activated Protein Kinase and JNK1/2/FoxO1 and AP-1 Pathways in Human Pulmonary Alveolar Epithelial Cells Leads to Up-Regulation of COX-2/PGE(2) Induced by Silica Nanoparticles. *Biomedicines* **2023**, *11*, 2628.
(35) Delaval, M.; Boland, S.; Solhonne, B.; Nicola, M.-A.; Mornet, S.; Baeza-Squiban, A.; Sallenave, J.-M.; Garcia-Verdugo, I. Acute exposure to silica nanoparticles enhances mortality and increases lung permeability in a mouse model of Pseudomonas aeruginosa pneumonia. *Part Fibre Toxicol.* **2015**, *12*, 1.
(36) Rabolli, V.; Badissi, A. A.; Devosse, R.; et al. The alarmin IL-1alpha is a master cytokine in acute lung inflammation induced by silica micro- and nanoparticles. *Part Fibre Toxicol.* **2014**, *11*, 69.
(37) Li, X.; Li, Y.; Lv, S.; Xu, H.; Ma, R.; Sun, Z.; Li, Y.; Guo, C. Long-term respiratory exposure to amorphous silica nanoparticles promoted systemic inflammation and progression of fibrosis in a susceptible mouse model. *Chemosphere* **2022**, *300*, 134633.
(38) Bartucci, R.; Paramanandana, A.; Boersma, Y. L.; Olinga, P.; Salvati, A. Comparative study of nanoparticle uptake and impact in murine lung, liver and kidney tissue slices. *Nanotoxicology* **2020**, *14*, 847−865.
(39) Inoue, M.; Sakamoto, K.; Suzuki, A.; et al. Size and surface modification of silica nanoparticles affect the severity of lung toxicity by modulating endosomal ROS generation in macrophages. *Part Fibre Toxicol.* **2021**, *18*, 21.
(40) Zhang, J.; Yang, X.; Yang, Y.; Xiong, M.; Li, N.; Ma, L.; Tian, J.; Yin, H.; Zhang, L.; Jin, Y. NF-κB mediates silica-induced pulmonary inflammation by promoting the release of IL-1β in macrophages. *Environ. Toxicol* **2022**, *37*, 2235−2243.
(41) Wijsenbeek, M.; Cottin, V. Spectrum of Fibrotic Lung Diseases. *N Engl J. Med.* **2020**, *383*, 958−968.
(42) Zhao, X.; Abulikemu, A.; Lv, S.; Qi, Y.; Duan, J.; Zhang, J.; Chen, R.; Guo, C.; Li, Y.; Sun, Z. Oxidative stress- and mitochondrial dysfunction-mediated cytotoxicity by silica nanoparticle in lung epithelial cells from metabolomic perspective. *Chemosphere* **2021**, *275*, 129969.
(43) Cui, H.; Xie, N.; Banerjee, S.; et al. CD38 Mediates Lung Fibrosis by Promoting Alveolar Epithelial Cell Aging. *Am. J. Respir Crit Care Med.* **2022**, *206*, 459−475.
(44) Kirk, T.; Ahmed, A.; Rognoni, E. Fibroblast Memory in Development, Homeostasis and Disease. *Cells* **2021**, *10*, 2840.
(45) Strieter, R. M.; Mehrad, B. New mechanisms of pulmonary fibrosis. *Chest* **2009**, *136*, 1364−1370.
(46) Petrache Voicu, S.; Dinu, D.; Sima, C.; Hermenean, A.; Ardelean, A.; Codrici, E.; Stan, M.; Zarnescu, O.; Dinischiotu, A. Silica Nanoparticles Induce Oxidative Stress and Autophagy but Not Apoptosis in the MRC-5 Cell Line. *Int. J. Mol. Sci.* **2015**, *16*, 29398−29416.
(47) Li, N.; Wang, L.; Shi, F.; et al. Silica nanoparticle induces pulmonary fibroblast transdifferentiation via macrophage route: Potential mechanism revealed by proteomic analysis. *Toxicol. In Vitro* **2021**, *76*, 105220.
(48) Bouchecareilh, M.; Balch, W. E. Proteostasis: a new therapeutic paradigm for pulmonary disease. *Proc. Am. Thorac Soc.* **2011**, *8*, 189−195.
(49) Kelsen, S. G. The Unfolded Protein Response in Chronic Obstructive Pulmonary Disease. *Ann. Am. Thorac. Soc.* **2016**, *13*, S138−S145.
(50) Smith, J. A. Regulation of Cytokine Production by the Unfolded Protein Response; Implications for Infection and Autoimmunity. *Front. Immunol.* **2018**, *9*, 422.
(51) Sonninen, T.-M.; Goldsteins, G.; Laham-Karam, N.; Koistinaho, J.; Lehtonen, S. Proteostasis Disturbances and Inflammation in Neurodegenerative Diseases. *Cells* **2020**, *9*, 2183.
(52) Miles, J.; Scherz-Shouval, R.; van Oosten-Hawle, P. Expanding the Organismal Proteostasis Network: Linking Systemic Stress Signaling with the Innate Immune Response. *Trends Biochem. Sci.* **2019**, *44*, 927−942.

https://doi.org/10.1021/envhealth.4c00052
Environ. Health 2024, 2, 786−801

(53) Shin, J. N.; Fattah, E. A.; Bhattacharya, A.; Ko, S.; Eissa, N. T. Inflammasome activation by altered proteostasis. *J. Biol. Chem.* **2013**, *288*, 35886−35895.
(54) Watanabe, S.; Markov, N. S.; Lu, Z.; et al. Resetting proteostasis with ISRIB promotes epithelial differentiation to attenuate pulmonary fibrosis. *Proc. Natl. Acad. Sci. U. S. A.* **2021**, *118*, e2101100118.
(55) Cui, X.; Zhang, Y.; Lu, Y.; Xiang, M. ROS and Endoplasmic Reticulum Stress in Pulmonary Disease. *Front. Pharmacol.* **2022**, *13*, 879204.
(56) Yun, C. W.; Kim, H. J.; Lim, J. H.; Lee, S. H. Heat Shock Proteins: Agents of Cancer Development and Therapeutic Targets in Anti-Cancer Therapy. *Cells* **2020**, *9*, 60.
(57) Tanguy, J.; Pommerolle, L.; Garrido, C.; Kolb, M.; Bonniaud, P.; Goirand, F.; Bellaye, P.-S. Extracellular Heat Shock Proteins as Therapeutic Targets and Biomarkers in Fibrosing Interstitial Lung Diseases. *Int. J. Mol. Sci.* **2021**, *22*, 9316.
(58) Mittal, S.; Rajala, M. S. Heat shock proteins as biomarkers of lung cancer. *Cancer Biol. Ther* **2020**, *21*, 477−485.
(59) Wang, L.; Zhao, H.; Zhang, L. HSP90AA1, ADRB2, TBL1XR1 and HSPB1 are chronic obstructive pulmonary disease-related genes that facilitate squamous cell lung cancer progression. *Oncol Lett.* **2020**, *19*, 2115−2122.
(60) Barone, R.; Marino Gammazza, A.; Paladino, L.; Pitruzzella, A.; Spinoso, G.; Salerno, M.; Sessa, F.; Pomara, C.; Cappello, F.; Rappa, F. Morphological Alterations and Stress Protein Variations in Lung Biopsies Obtained from Autopsies of COVID-19 Subjects. *Cells* **2021**, *10*, 3136.
(61) Richter, K.; Haslbeck, M.; Buchner, J. The heat shock response: life on the verge of death. *Mol. Cell* **2010**, *40*, 253−266.
(62) Zhu, Y.; Lu, X.; Wu, D.; Cai, S.; Li, S.; Teng, X. The effect of manganese-induced cytotoxicity on mRNA expressions of HSP27, HSP40, HSP60, HSP70 and HSP90 in chicken spleen lymphocytes in vitro. *Biol. Trace Elem. Res.* **2013**, *156*, 144−152.
(63) Alderson, T. R.; Roche, J.; Gastall, H. Y. Local unfolding of the HSP27 monomer regulates chaperone activity. *Nat. Commun.* **2019**, *10*, 1068.
(64) Oh, A.; Jeon, S.; Jeong, M. G.; Kim, H. K.; Kang, J.; Lee, Y.-S.; Hwang, E. S. HSPB1 inhibitor J2 attenuates lung inflammation through direct modulation of Ym1 production and paracrine signaling. *Biomed. Pharmacother.* **2021**, *143*, 112225.
(65) Kim, J. Y.; Jeon, S.; Yoo, Y. J.; et al. The Hsp27-Mediated IkBalpha-NFkappaB Signaling Axis Promotes Radiation-Induced Lung Fibrosis. *Clin. Cancer Res.* **2019**, *25*, 5364−5375.
(66) Kampinga, H. H.; Craig, E. A. The HSP70 chaperone machinery: J proteins as drivers of functional specificity. *Nat. Rev. Mol. Cell Biol.* **2010**, *11*, 579−592.
(67) Gu, J.; Liu, Z.; Zhang, S.; et al. Hsp40 proteins phase separate to chaperone the assembly and maintenance of membraneless organelles. *Proc. Natl. Acad. Sci. U. S. A.* **2020**, *117*, 31123−31133.
(68) Kastenhuber, E. R.; Lalazar, G.; Houlihan, S. L.; et al. DNAJB1-PRKACA fusion kinase interacts with beta-catenin and the liver regenerative response to drive fibrolamellar hepatocellular carcinoma. *Proc. Natl. Acad. Sci. U. S. A.* **2017**, *114*, 13076−13084.
(69) Bascos, N. A. D.; Mayer, M. P.; Bukau, B.; Landry, S. J. The Hsp40 J-domain modulates Hsp70 conformation and ATPase activity with a semi-elliptical spring. *Protein Sci.* **2017**, *26*, 1838−1851.
(70) Pei, Q.; Ni, W.; Yuan, Y.; Yuan, J.; Zhang, X.; Yao, M. HSP70 Ameliorates Septic Lung Injury via Inhibition of Apoptosis by Interacting with KANK2. *Biomolecules* **2022**, *12*, 410.
(71) Caruso Bavisotto, C.; Alberti, G.; Vitale, A. M.; et al. Hsp60 Post-translational Modifications: Functional and Pathological Consequences. *Front. Mol. Biosci.* **2020**, *7*, 95.
(72) Saibil, H. Chaperone machines for protein folding, unfolding and disaggregation. *Nat. Rev. Mol. Cell Biol.* **2013**, *14*, 630−642.
(73) Kumar, S.; O'Malley, J.; Chaudhary, A. K.; Inigo, J. R.; Yadav, N.; Kumar, R.; Chandra, D. Hsp60 and IL-8 axis promotes apoptosis resistance in cancer. *Br. J. Cancer* **2019**, *121*, 934−943.
(74) Sangiorgi, C.; Vallese, D.; Gnemmi, I.; et al. HSP60 activity on human bronchial epithelial cells. *Int. J. Immunopathol. Pharmacol.* **2017**, *30*, 333−340.
(75) Ou, G.; Zhu, M.; Huang, Y.; et al. HSP60 regulates the cigarette smoke-induced activation of TLR4-NF-kappaB-MyD88 signalling pathway and NLRP3 inflammasome. *Int. Immunopharmacol.* **2022**, *103*, 108445.
(76) Cappello, F.; Caramori, G.; Campanella, C.; et al. Convergent sets of data from in vivo and in vitro methods point to an active role of Hsp60 in chronic obstructive pulmonary disease pathogenesis. *PLoS One* **2011**, *6*, No. e28200.
(77) Quintana, F. J.; Cohen, I. R. The HSP60 immune system network. *Trends Immunol* **2011**, *32*, 89−95.
(78) von Hertzen, L. C. Role of persistent infection in the control and severity of asthma: focus on Chlamydia pneumoniae. *Eur. Respir. J.* **2002**, *19*, 546−556.
(79) Schopf, F. H.; Biebl, M. M.; Buchner, J. The HSP90 chaperone machinery. *Nat. Rev. Mol. Cell Biol.* **2017**, *18*, 345−360.
(80) Solopov, P.; Colunga Biancatelli, R. M. L.; Marinova, M.; Dimitropoulou, C.; Catravas, J. D. The HSP90 Inhibitor, AUY-922, Ameliorates the Development of Nitrogen Mustard-Induced Pulmonary Fibrosis and Lung Dysfunction in Mice. *Int. J. Mol. Sci.* **2020**, *21*, 4740.
(81) Sontake, V.; Wang, Y.; Kasam, R. K.; et al. Hsp90 regulation of fibroblast activation in pulmonary fibrosis. *JCI Insight* **2017**, *2*, No. e91454.

NOTE ADDED AFTER ASAP PUBLICATION

This paper was published on July 1, 2024. A unit of measurement was corrected in section 2.1, and the paper was reposted on October 23, 2024.

https://doi.org/10.1021/envhealth.4c00052
Environ. Health 2024, 2, 786−801